FERMILAB-CONF-06-102-AD

# APPLICATIONS OF BARRIER BUCKET RF SYSTEMS AT FERMILAB*

C. M. Bhat
Fermilab, P.O. Box 500, Batavia, IL, 60510, U.S.A.

*Abstract*

In recent years, the barrier rf systems have become important tools in a variety of beam manipulation applications at synchrotrons. Four out of six proton synchrotrons at Fermilab are equipped with broad-band barrier rf systems. All of the beam manipulations pertaining to the longitudinal phase space in the Fermilab Recycler (synchrotron used for antiproton storage) are carried out using a barrier system. Recently, a number of new applications of barrier rf systems have been developed- the longitudinal momentum mining, longitudinal phase-space coating, antiproton stacking, fast bunch compression and more. Some of these techniques have been critical for the recent spectacular success of the collider performance at the Fermilab Tevatron. Barrier bunch coalescing to produce bright proton bunches has a high potential to increase proton antiproton luminosity significantly. In this paper, I will describe some of these techniques in detail. Finally, I make a few general remarks on issues related to barrier systems.

## CONTENTS



## I. INTRODUCTION

During the early stages of the Tevatron project [1] at Fermilab it was highly essential to develop a technique to preserve a gap of about 110 nsec in the de-bunched antiproton beam in the Fermilab Debuncher for efficient beam stacking and produce an isolated antiproton bunch in the Accumulator at the time of beam transfer to the Tevatron for collider operation. This led to the development of barrier rf technology [2]. Since then, a number of high energy physics labs around the world have used barrier rf systems in circular accelerators and investigated their applications [3-20]. The Recycler at Fermilab, a 8 GeV antiproton storage ring, uses a barrier rf system in all of its beam manipulations unlike any previously built storage rings in the past.

A barrier rf system is a broad-band rf system comprising of ferrite loaded rf cavities. The modern barrier rf systems have operating bandwidth in the range of tens of kHz to hundreds of MHz. A barrier rf wave is generated by wide-band solid state power amplifiers. For example, the Recycler rf system comprise of four 50 Ω cavities each driven by 3500A100 solid state amplifiers [21]. This can be operated in the frequency range of 10kHz -100MHz. Unlike in a resonant rf system, one can produce an arbitrary voltage wave form between gaps of a barrier rf cavity. Fig. 1 shows an example of rf voltage waveform produced by Recycler rf system. Azimuthally, there are three rectangular rf buckets of different widths and four sinusoidal wave of 2.5 MHz.

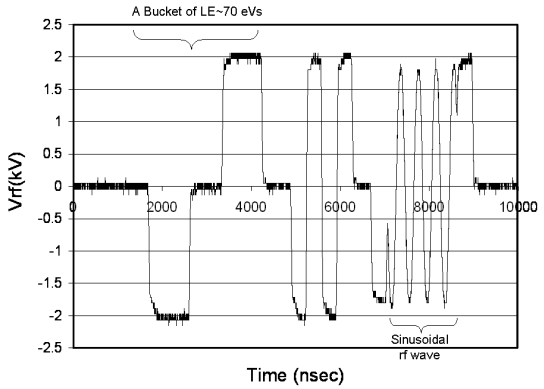


Fig. 1: A typical example of a complicated rf wave form generated at the rf gaps of the Fermilab Recycler barrier rf cavity. The data shown is for about 90% of the ring.

One can also generate some specific wave forms using fast switches [22].

An rf system is used to control the longitudinal dynamics of the beam particles in an accelerator. Preservation of the longitudinal emittance (LE) during any rf manipulation is quite important. In most of the proton synchrotrons the transverse and longitudinal motions are uncoupled. Consequently, any beam gymnastics with rfs have little effect on the transverse motions of the beam particles.

In this section, I compile some important features of different barrier rf systems at Fermilab and their utilization. Next, an overview of the longitudinal beam dynamics in barrier rf buckets is given. Finally, different methods for longitudinal emittance measurements used at Fermilab Recycler and their limitations are outlined. In

*Operated by Universities Research Association, Inc. for the U.S. Department of Energy under contract DE-AC02-76CH03000.
#cbhat@fnal.gov

the rest of the paper emphasis is given on applications of barrier rf systems in the Recycler and the Main Injector [23].

### 1. Barrier rf Systems at Fermilab

There are many barrier rf systems in use at Fermilab synchrotrons- the antiproton Accumulator, Debuncher [1], Recycler [4] and very recently in the 150 GeV Main Injector (MI) [20, 22]. The approximate locations of the barrier rf cavities in the rings are shown in Fig. 2. Each one of them is used for a different purpose. The general properties of these barrier rf systems and their functions are summarized in Table 1.

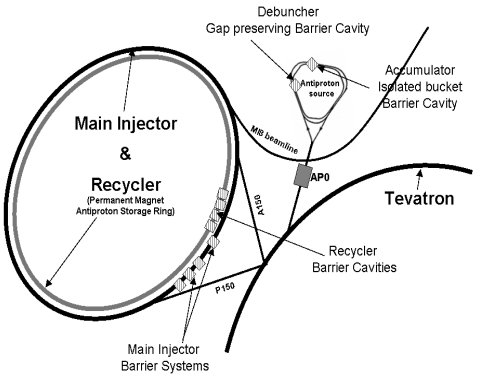


Fig. 2: The barrier rf systems in the Fermilab accelerator complex. The Main Injector (8-150 GeV accelerator) and the Recycler (permanent magnet 8 GeV storage ring) share the same underground tunnel, and, have the same circumferences. Similarly, the anti-proton Debuncher and the Accumulator (both are storage rings) share another tunnel, but, have different circumferences.

### 2. An overview of longitudinal beam dynamics of barrier buckets and some useful formulae

The motion of any particle with energy $\Delta E$ relative to the synchronous particle with energy $E_0$ in a synchrotron is given by [24],

$$\frac{d\tau}{dt} = -\eta \frac{2\pi \Delta E}{T_0 \beta^2 E_0} \quad \text{and} \quad \frac{d(\Delta E)}{dt} = \frac{eV(\tau)}{T_0} \tag{1}$$

The quantities $\eta$, $T_0$ and $\beta$ are phase slip factor, the revolution period and the ratio of the particle velocity to that of velocity of light, respectively. $-\tau$ is the time difference between the arrival of this particle and that of a synchronous particle at the centre of the rf bucket. $V(\tau)$ is the amplitude of the rf voltage wave-form. Using the above equations, one can construct the Hamiltonian for synchrotron motion of the particle, given by,

Table 1: Barrier rf systems at Fermilab

| **Accelerator/ Storage ring & Function of Barrier rf Sysm.** | **Ferrite Type (Cavity Dimension)** | **Properties (Power, $V_{peak}$, $R_{shunt}$, Band-width, Power Amplifiers)** |
|---|---|---|
| Debuncher – Gap preserving | MnZn+NiZn (~ 1 meter) | 2.4kW, 700V, 104Ω, 10kHz-10MHz,IFI3100S [1,2] |
| Accumulator – Ion clearing and isolated bucket | MnZn+NiZn (~1 meter) | 100W, 70V, 50Ω, 10kHz-10MHz, ENI2100 [1,2] |
| Recycler – for all rf manipulations | Ceramic Magnetics MN60, CMD10 (~1 meter) | 4×3.5kW, 4×500V, 4×50Ω , 10kHz-100MHz, Amplifier Research Model 3500A100 [4,21] |
| MI – Test cavity | Finemet®core (~0.75 meter) | 150kW, 10kV, 500Ω Fast Switch [22] |
| MI – Damper Cavities | MnZn+NiZn (~1 meter) | 3×3.5kW, 3×500V, 3×50Ω , 10kHz-100MHz, Amplifier Research Model 3500A100 [21] |

$$H(\tau, \Delta E) = -\frac{\eta}{2\beta^2 E_0}\Delta E^2 - \frac{e}{T_0}\int_0^{\tau} V(t)dt \tag{3}$$

We identify the second term of the above equation as the potential energy $U(\tau)$ of the particles, given by,

$$U(\tau) = -\frac{e}{T_0}\int_0^{\tau} V(t)dt. \tag{4}$$

In most part of this article we will deal with rectangular barrier buckets. For a rectangular barrier bucket, $V(t)$ is given by,

$$V(t) = \begin{cases} -V_0 \ for -T_1 - T_2/2 \le t < -T_2/2 \\ 0 \quad for -T_2/2 \le t < T_2/2 \\ V_0 \quad for\, T_2/2 \le t < T_1 + T_2/2 \end{cases} \tag{5}$$

where $T_1$ and $T_2$ denote barrier pulse width and gap between rf pulses. A schematic view of particle beam phase space distribution in a rectangular rf wave in a storage ring operating below *transition energy* is shown in Fig.3. The particle density is maximum in the vicinity of synchronous particles, for a cold beam.

The relationship between half bucket height and the corresponding voltage waveform is given by,

$$\Delta E_b = \sqrt{\frac{2\beta^2 E_0}{|\eta|}\frac{\left|\int_{T_2/2}^{T_2/2+T_1} eV(\tau)d\tau\right|}{T_0}} \qquad (6)$$

Since the bucket height depends upon $\int eV(\tau)d\tau$, the exact shape of the wave form is not very critical as long as it had some symmetry about the bucket centre.

The beam half energy spread $\Delta \hat{E}$ and its penetration $\hat{T}_1$ into the barrier are given by,

$$\Delta \hat{E} = \sqrt{\frac{2\beta^2 E_0}{|\eta|}\frac{eV_{rf}\hat{T}_1}{T_0}} \qquad (7)$$

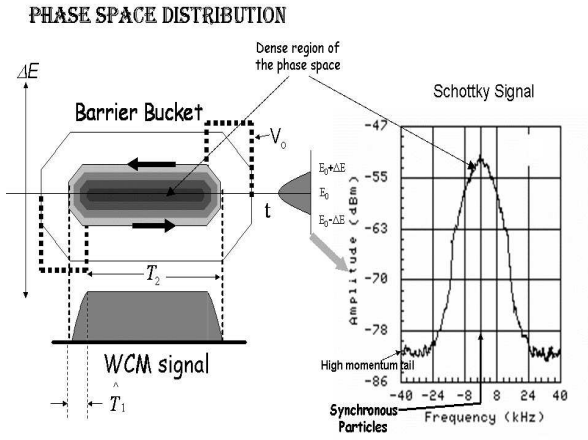


Fig. 3: A schematic of a rectangular barrier rf bucket is shown by dark dashed-line in the left picture. The bounded contour represents the bucket and the filled area shows beam in the barrier bucket. A schematic of resistive wall current monitor (WCM) signal of the beam is shown in the bottom picture. The beam penetration into the barrier pulse is "$\hat{T}_1$". On the right side a typical energy spectrum measured using a Schottky detector is shown.

The longitudinal emittance $\varepsilon_l$ of the beam in a rectangular barrier bucket is given by,

$$\varepsilon_l = 2T_2\Delta\hat{E} + \frac{8\pi|\eta|}{3\omega_o\beta^2 E_o eV_o}\Delta\hat{E}^3 \qquad (8)$$

where $\omega_0 = 2\pi/T_0$. The synchrotron oscillation period for particles with energy deviation $\Delta\hat{E}$ is given by,

$$T_s = \frac{2T_2}{|\eta|}\frac{\beta^2 E_o}{\left|\Delta\hat{E}\right|} + \frac{4\left|\Delta\hat{E}\right|T_0}{eV_o} \qquad (9)$$

## 3. Measurement of Longitudinal Emittance

The knowledge of correct longitudinal emittance is key to the understanding of the longitudinal beam dynamics. An accurate measurement of longitudinal emittance of particle beams in a synchrotron is not a trivial task. We have explored four different longitudinal emittance measurement techniques [13] in the Recycler. Two of them are destructive and two are non-destructive techniques. Here, I outline the general principles and their limitations of two non-destructive methods.

### *i. Wall Current Monitor (WCM)*

A WCM measures the image charge that flows along the vacuum chamber following the beam and reproduces the longitudinal profile of the beam. A schematic view of the WCM data for beam in the Recycler is shown in Fig. 3. By knowing the location of the barrier pulses and their shapes relative to the WCM signals one can measure the beam penetration into the barrier pulse. Using Eqs. (7) and (8), one can estimate the $\Delta\hat{E}$ and the longitudinal emittance of the beam. For a beam confined in a symmetric rectangular barrier bucket the beam penetration is symmetric with respect to the center of the bunch. However, any asymmetry in the shape of the pulse or non-zero rf voltage in the gap between barrier pulses (which might arise due to high-level or low-level rf issues), or, beam-loading effects [25] or, contributions from all of these give rise to an asymmetric beam penetration in the barriers. Then, one needs to adopt Monte-Carlo method [13] to estimate the longitudinal emittance.

The Recycler has a WCM with 4 GHz band width [26]. Signals from the WCM are sent to a fast digitizing scope RDT720 or LeCroy scope. The rf fan-out signals are also processed along with the WCM signals to measure the relative position of the barrier pulse in the ring. The data is collected using a software program [27] for later analysis. Several examples of the WCM data are shown in later sections.

### *ii. Longitudinal Schottky Detectors*

Use of Schottky signals for beam energy spread measurement in a storage ring is rather old and an elegant method [28]. For a coasting beam, the energy spread $\Delta\hat{E}$ and the frequency spread of the Schottky spectrum $\Delta f$ are related according to

$$\frac{\Delta\hat{E}}{E_0} = \frac{\beta^2}{\eta}\frac{\Delta f}{f_0} \qquad (10)$$

where $f = nf_0$, $f_0 = 1/T_0$, is the revolution frequency of the synchronous particles and $n$ is the harmonic number of the longitudinal Schottky signals. It can be shown that if the harmonic number "$n$" is selected sufficiently high then, Eq. (10) is still valid in the case of a bunched beam.

The Recycler has two longitudinal Schottky detectors; one with $n \approx 19500$ (1.75 GHz detector) [29] and the second has $n = 882$ (79 MHz detector).

The Schottky measurements do not depend on barrier shape, baseline issues etc. In conjunction with the measured $T_2$ one can estimate the emittance of the beam fairly accurately. For antiprotons in the Recycler cooled using stochastic cooling technique, the energy distribution resembles Gaussian distribution. Then, the relation between measured rms energy spread, "$\sigma_{rms}$" from a Schottky detector and the 90% longitudinal emittance is given by[30],

$$\varepsilon_l(90\ \%) = C_1 T_2 \sigma_{rms} + C_2 \sigma^3_{rms} + C_3 \frac{\sigma^4_{rms}}{\sqrt{T_2}} \qquad (11)$$

The constants $C_1$, $C_2$, and $C_3$, are 3.29, 0.064 and 1/325.4, respectively. The $\sigma_{rms}$ is rms energy spread of the beam particle distribution in units of "MeV" and $T_2$ in units of "μsec". Note that this expression is good within ±0.4% for $\sigma^2_{rms}/T_2 < 100$ MeV$^2$/μsec. This expression is modified to estimate the 95% emittance.

One of the assumptions in using the Schottky signals for the measurements of beam energy spread is that signals do not saturate and do not have coherent signals. The later one is difficult to detect. Care should be taken to eliminate these problems.

### *iii* The *Uncertainties in Measured Longitudinal Emittance*

The uncertainty in the measured longitudinal emittance from the WCM signals depend upon the accuracy of measurement of $\hat{T}_1$. The scope resolution, cable dispersion and WCM responses to the beam play very important role here. Besides, there are a few additional sources of errors in the measured emittance from the WCM data.

1. Uncertainty in waveform: knowing the accurate shape of the rf wave form in emittance measurements is quite important. While using the formulae (7) and (8) one assumes ideal rectangular wave form. In reality, the rf wave forms are not perfect rectangular in shape (see for example Fig.1). This might introduce significant uncertainties in the measured emittance based on deviation of measured rf pulse shape from that of ideal shape. For example, in case of Recycler, a bunch with LE=1 eVs in a rectangular barrier bucket of $V_o$ = 2 kV and $T_2$ =0.0 nsec, the expected $\hat{T}_1 \approx 72$ nsec. If there is a slope of 0.05kV/nsec at zero crossing (instead of slope being infinity), one overestimates the emittance of the beam by 60%. This uncertainty becomes smaller for larger emittance beam (uncertainty of 5% for a 22 eVs bunch).
2. The uncertainty in amplitude of the measured rf wave and beam-loading effects. The later makes the beam distribution asymmetric in a barrier buckets with $T_2 \neq 0.0$.
3. Use of designed lattice parameters in emittance calculations is another source of uncertainty. For example, error in measured $\eta$ is generally more than 10%.

Therefore, we arbitrarily assign a minimum of 20% error in the final measured emittance from WCM data. However, the measurements of relative emittance can be done fairly correctly and is very useful in some beam dynamics studies.

Measurement of the energy spread with Schottky detectors is quite accurate but, is very slow. One can expect the accuracy in the measured energy spread <5%. Emittance measurements using Eq. (11) assumes Gaussian distribution in energy coordinates. This may not be the case for a newly injected beam or e-cooled beam [31].

Therefore, we use both WCM and Schottky data, wherever possible, to establish the final longitudinal emittance and $\Delta\hat{E}$ of the beam.

## II. BEAM DYNAMICS SIMULATIONS

Every stage of the beam rf manipulation presented here is simulated using 2D beam dynamics tracking code ESME [32]. This code has been widely used around the world to understand the longitudinal beam dynamics in circular accelerators and predicts observed phenomenon. The space-charge and wake-field effects can also be modelled in the simulation.

Early on in our studies on the Recycler it was realized that various rf gymnastics needed for its operation, like beam stacking, cooling and unstacking etc., can be organized into sequences of a few basic steps. These steps involve process like injection, bunch compression, bunch expansion, cogging of a large bunch around the ring, bunch merging etc. [10, 18]. Therefore, simulations were carried out in two steps. The first step involves an optimization of individual steps with an emphasis on preservation of longitudinal emittance. Second step involves full simulations of stacking and un-stacking processes under different scenario.

During these simulations, importance is given about modeling the initial beam distribution. For example, anti-proton beam distribution resulted from stochastic cooling resembles Gaussian in energy. On the other hand, newly injected beam matched to a rf bucket resembles a parabolic distribution. Therefore, care is taken to model properly while simulating a process.

## III. PIECEWISE BEAM MANIPULATIONS WITH BARRIER RF SYSTEM

The beam tests are carried out first on basic steps mentioned above in the Recycler by varying beam intensities and initial longitudinal emittance. The studies guided us to bench-mark each step. Finally they are put together to form a complete sequence. For example, a complete stacking sequence in the Recycler comprises of

i. injecting antiprotons from MI to the Recycler in matched 2.5MHz rf buckets,

ii. de-bunching the injected beam in a barrier bucket without emittance growth,

iii. compressing or stretching the distribution to match the $\Delta \hat{E}$ to already existing stack,

iv. merge the newly injected beam to the existing stack without emittance growth.

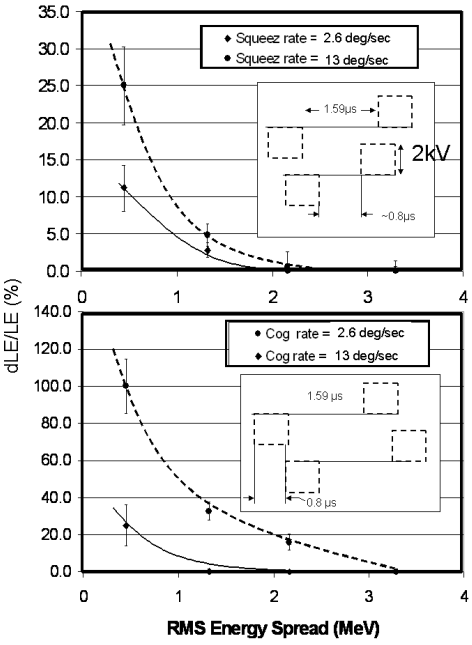


Fig. 4: ESME simulation of predicted longitudinal emittance growth vs beam RMS energy spread for two different compression rates (top) (symmetric compression) and for two cog rates (bottom). These simulations are carried out for beam in rectangular barrier buckets of $T_2$=1.59μsec. The curves are drawn to guide the eye.

The bunch compression and cogging is accomplished by slowly changing the phase of the barrier pulses relative to a fixed point. Fig. 4 shows the results from simulations of bunch squeezing and bunch cogging with a parabolic particle distribution in ($\Delta$E, $\tau$)-phase space. A barrier bucket with $V_0$ = 2 kV and $T_1$ = 0.903 μsec and $T_2$ = 1.59μsec are used.

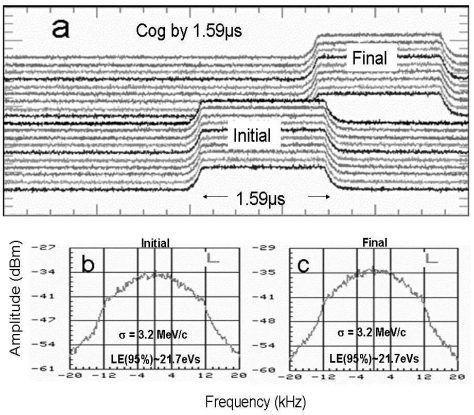


Fig. 5: Experimental measurements on beam cogging in the Recycler. A beam bunch of width≈1.59μsec and beam intensity ~40E10 p (a) WCM data for cogging rate of 2.97deg/sec (b) the Schottky energy spectrum before cogging and (c) after the cogging. The measured energy spreads and 95% longitudinal emittance from the Schottky data are also shown.

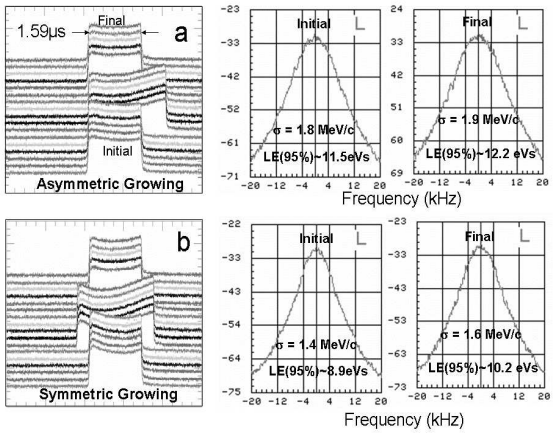


Fig. 6. Experimental data on growing and compression of a bunch of width≈1.59μsec (a) WCM data for non-symmetric growing, corresponding Schottky data for initial and final beam distributions (beam intensity ~45E10 p) (b) similar data for symmetric growing and shrinking (beam intensity ~47E10 p). The measured energy spreads and 95% longitudinal emittance from the Schottky data are also shown. Barrier cog rate = 2.97deg/sec.

The particles in a rectangular barrier bucket with different energy spreads have different synchrotron oscillation frequency according to Eq. (9). The particles closer to the synchronous energy have smaller oscillation period as compared with the one farther. Therefore, criteria for adiabatic bunch rf manipulations

will be different for particles with different $\Delta\hat{E}$. The simulations clearly demonstrate a strong dependence of emittance growth during bunch compression and cogging as a function of $\Delta\hat{E}$. It is important to note that the results shown in Fig. 4 can not be used for a barrier bucket of arbitrary $T_2$ and other parameters. Simulations have to be repeated on case by case basis. However, the results shown here are merely representative.

At present, the Recycler LLRF capability for different beam gymnastics is quite versatile [33]. The barrier pulses can be moved azimuthally at three different cog rates – 2.97degs/sec (slow), 7.34 deg/sec (medium) and 5142 deg/sec (fast). Fig. 5 shows the experimental results on cogging on proton beam with fairly large $\Delta\hat{E}$. The speed was chosen to be 2.97deg/sec. Within the errors of measurements we did not see any emittance growth. The ESME predictions are consistent with this finding.

Fig. 6 shows data on symmetric as well as asymmetric bunch compression and growth. The initial energy spreads for these experiments are chosen to be $\Delta\hat{E}$= 1.4 MeV and 1.8 MeV, respectively. The Schottky measurements after beam stretching and compression indicate emittance growths.

The Main Injector is a multi-purpose 8-150 GeV accelerator and its acceleration ramps have significant effect on the longitudinal emittance of the Recycler beam [11, 34]. Over the years a ramp compensation correction scheme has been developed and implemented in the Recycler [35]. During beam studies presented in Fig. 5 and 6 we had the compensation on, but not fully optimized. Observed emittance growths which are likely from the Main Injector ramp effect are not explained by the ESME predictions shown in Fig. 4. However, the experiments carried out on the e-cooled beam with full ramp compensation support the findings from the ESME simulations.

# IV NOVEL BEAM MANIPULATION TECHNIQUES

## a. Beam stacking in the Recycler

Achieving high intensity cold antiproton stacks, emittance preservation and un-stacking them from the Recycler are critical for the success of the Run II [36] at the Tevatron. The design goal for the antiproton stack in the Recycler is about $600\times10^{10}$ and it takes about 20-30 hr to build up this stack. At the end, the entire stack is transferred to the Tevatron for collider operation.

The antiprotons are produced by colliding high intensity 120 GeV protons on a solid metallic target. They are primarily stored and cooled in the Fermilab Accumulator Ring [1]. As the stack size in the Accumulator increases the accumulation rate decreases significantly. Therefore, we empty the Accumulator by transferring antiprotons to the Recycler very often. At the start of each transfer the longitudinal emittance of the antiprotons in the Accumulator is about 25 eVs (and transverse emittance is about 10-12π mm-mr). However, the present method of un-stacking from the Accumulator, "traverse momentum mining", gives rise to emittance growth by a factor of three.

The stacking of antiproton in the Recycler is carried out azimuthally. Most of these transfers are carried out in the presence of cooled antiprotons. To make the stacking process very efficient, it is essential to minimize the emittance growth of the stacked antiprotons in the Recycler during stacking.

The beam stacking in the Recycler has evolved over the years. New methods have been invented to make antiproton stacking more adiabatic. Some of these methods are discussed below.

### *i. Past and present antiproton stacking schemes*

A schematic view of a technique used from 2001-2005 [18, 37] and the one in use currently [38] are shown in Fig. 7.

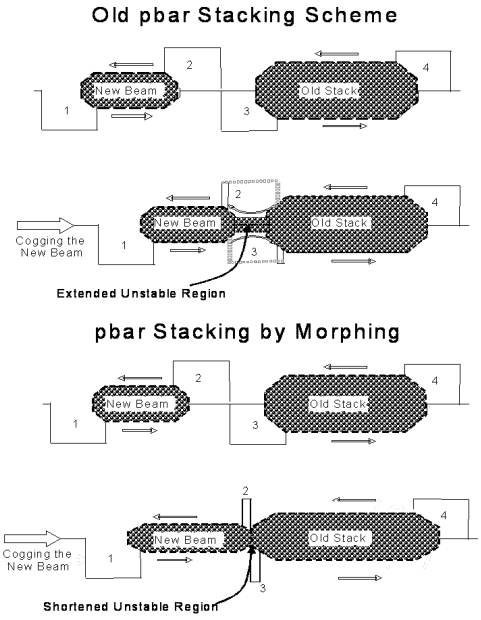


Fig. 7: Schematic view of antiproton stacking schemes in the Recycler, (a) past and (b) present- morphing technique. Four rectangular barrier pulses are indicated by numbers 1, 2, 3 and 4. The phase-space distribution of the new and cold stacks and, their synchrotron motion (arrows) are indicated between barriers.

Four 2.5 MHz bunches with a maximum of 3.4 eVs each are injected into the Recycler via the Main Injector. Subsequently, these bunches are debunched in about 20 sec between two rectangular barrier pulses "1" and "2" to form "New Beam". This beam is merged with the "Cold Beam". In the old stacking method, the +ve barrier "2" is moved over the –ve barrier "3" slowly so that they cancel

out and beam particles move to merge together. However, the problem with this technique is that as barrier "2" moves over the barrier "3" an unstable region will be created and longitudinal emittance growth unavoidable. Beam studies showed about 100% emittance growth. The emittance growth is partly due to mis-match in energy spreads of new and cold stacks. This method of stacking limited us increasing the antiproton stack in the Recycler > $300\times10^{10}$ and cool them efficiently.

Recently we have implemented a better stacking scheme which involves "morphing" of barrier rf pulses [38]. In this case, the barrier pulses "2" and "3" slowly change their width according to some pre-determined rate set by Recycler LLRF program. This eliminates the extended unstable region as shown above in Fig. 7. The emittance growth is found to be as low as 15%. After implementation of this technique, we have stacked in excess of $430\times10^{10}$ antiprotons and continue cooling efficiently.

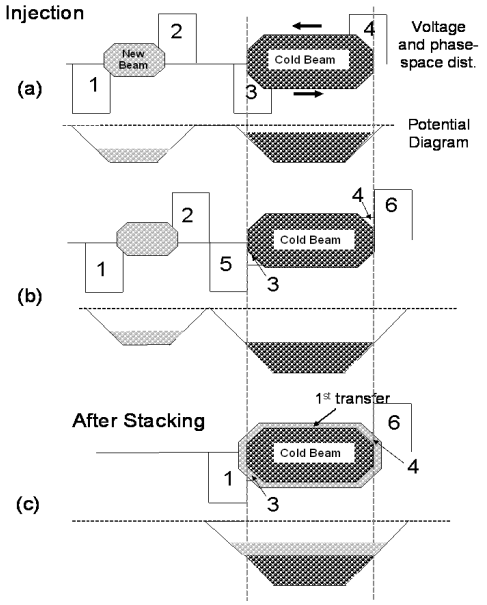


Fig. 8: Schematic view of the longitudinal phase-space coating. The phase space and potential diagrams (a) beam injection, (b) intermediate stage of lowering the potential energy of the cold beam relative to the injected beam, (c) after stacking. The voltage wave forms are also shown in each case.

### *ii. Longitudinal Phase-space Coating [39]*

In the antiproton stacking methods explained above, the cold beam was disturbed every time a new beam is merged. In the case of multiple transfers, the final emittance growth of the cold core is significant. In view of this a further attempt has been made to improve the stacking scheme.

In the past, antiproton stacking in the Recycler without longitudinal emittance growth is suggested [40]. This method also depends on how well the momentum spreads of the new and the cold beam stacks are matched before merging. The technique of longitudinal phase-space coating explained here, however, does not need matching of energy spreads before merging.

The method of "longitudinal phase-space coating" is different from "longitudinal phase-space painting" explained in literature [41]. This technique is first of its kind.

The principle of phase-space coating is illustrated schematically in Fig. 8. The important aspect of coating is that, after the injection one need to raise the potential of the new stack relative to the cold stack so that the bottom of the new stack levels with the top of the cold stack as shown in Fig.8(b). Subsequently, the rf pulses 2 and 5 are removed adiabatically and new beam is smeared on the outer most layer (in energy) of the cold stack without disturbing the core of the cold beam.

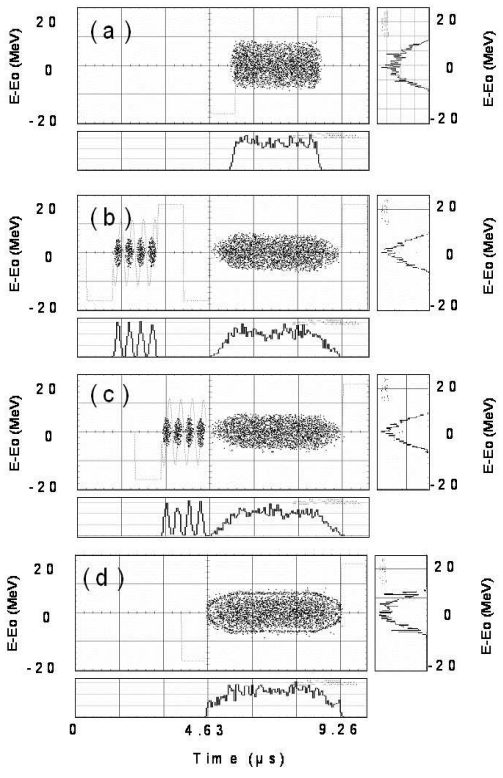


Fig. 9: ESME simulations of longitudinal phase-space coating in the Recycler. The ($\Delta E$, $\tau$)-phase space distributions, energy projection and predicted WCM data are shown at a) for cold beam distribution, b) after injection of four 2.5 MHz bunches, c) intermediate stage of coating and d) newly coated beam on the cold stack.

Fig. 9 shows the results from the ESME simulations of longitudinal phase space coating in the Recycler. The

longitudinal emittance of the cold beam is taken to be about 58 eVs and captured between two barriers with $V_0$= = 2 kV, $T_1$ = 0.908 μsec, $T_2$ = 2.84 μsec. The beam height of such beam was about 9.2 MeV. The simulations are used essentially to guide the experiments in the Recycler.

Before the first injection of the beam, the barrier pulse height of the cold beam is reduced from 2 kV to 300 V so that the bucket height is same as that of the beam (Fig. 9b). In principle this matching can also be obtained by reducing the width of the barrier pulses defining the boundary of the cold beam from 0.908 μsec to 0.227 μsec. Because of the present limitations of the Recycler LLRF, we had to follow the former way of matching.

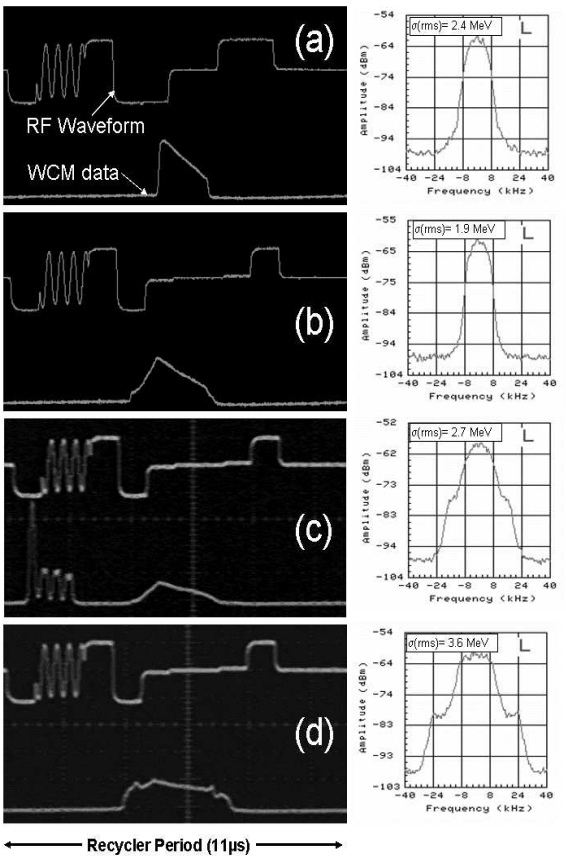


Fig. 10: Experimental data for longitudinal phase-space coating in the Recycler. Shown left are scope traces and on the right are the corresponding Schottky data. The top trace in each of the scope trace is the rf "fanback" (signals from rf gap monitors) signals, similar to the one shown in Fig.1. The lower trace is WCM data. a) for cold beam distribution, b) after matching the distribution by lowering the rf voltage, c) injection of four 2.5 MHz bunches, d) newly coated beam on the cold stack. The time is along the horizontal direction. The data covers one complete period of Recycler of 11.11 μsec.

Fig. 9b shows conditions after the new beam injection. The incoming beam is about 10 eVs (2.5 eVs × 4 bunches). This beam is coated on the old stack. The predicted energy spectrum shown in Fig.9d clearly shows two sharp peaks around the central peak. The simulations show no emittance growth in the cold beam even with multiple injections.

Fig. 10 shows the experimental data for the longitudinal phase space coating. There is noticeable difference between the predicted and the measured WCM data (for example see the Fig.10a). The causes for this discrepancy will be explained in Section V. Experimentally, all of the predicted features are seen. The detailed data analysis is in progress.

### b. Longitudinal Momentum Mining [16]

Necessity for an efficient method of cold antiproton beam extraction from the Recycler without longitudinal emittance growth for the Tevatron collider operation led to the invention of the longitudinal momentum mining. Presently, the steps involved in transferring antiprotons from Recycler to the Tevatron are, 1) divide the cold beam in to 36 smaller bunches and send them to the Main Injector (this is done in nine separate transfers with four bunches at a time) 2) accelerate them from 8 GeV to 150 GeV and transfer to the Tevatron. During the rf manipulation and acceleration in the Main Injector the antiprotons with energy spread larger than the momentum acceptance will be lost. Therefore, it is beneficial for antiproton economy to save these antiprotons in high momentum tail (indicated in the Schottky spectrum in Fig. 3) in the Recycler. Prior to the development of longitudinal momentum mining technique we had a method which simply sliced the cold antiproton distribution nine times along the time axis using another barrier bucket. This led to enormous emittance growth in longitudinal phase space, larger than that observed in transverse momentum mining in the Accumulator. In addition, the later transfers suffer from lower bunch intensity and larger LE (leading to more antiproton loss in the Main Injector). An efficient antiproton unstacking scheme was essential for the success of the Recycler.

The general principle of the longitudinal momentum mining is illustrated in Fig. 11. A schematic view of the rf wave form with beam phase space boundary (dashed lines in left figure) and the corresponding potential well, containing beam particles are shown. The objective of longitudinal momentum mining is to isolate particles closer to $E_o$ from the rest. This is accomplished by adiabatically inserting a set of mining buckets (in this illustration the number of mining buckets are selected to be three). The size of each mining bucket is chosen to be exactly same as what is needed later. The particles which can not be bound by these "mini" barriers are still bound by the larger barriers (Fig.11b) and executing synchrotron oscillations at a relatively higher rate than the one captured in the mini-barriers. Finally, the un-captured particles are isolated in another rf bucket as shown in Fig.

11c. Thus, are the particles with low longitudinal emittance are mined while leaving the rest.

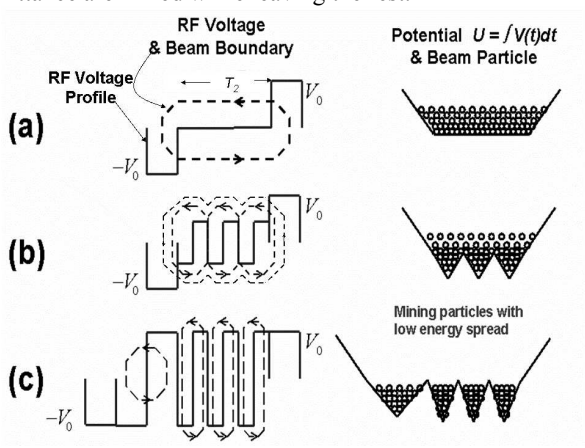


Fig. 11: Schematic view of the longitudinal momentum mining using barrier buckets. Barrier rf voltage (solid-lines) and beam particle boundary in ($\Delta E$, $\tau$)-phase space (dashed line) are shown on the left. The cartoons on the right show the potential well and the beam particles in it. (a) The initial distribution, (b) after confining particles with low energy spread in three mini buckets and (c) after isolating particles with high and low energy spreads.

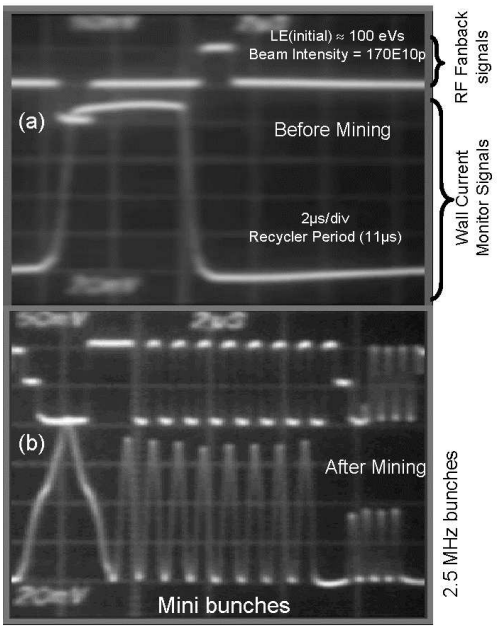


Fig. 12: The experimental data on longitudinal momentum mining in the Recycler with proton beam a) before mining, b) after mining. Horizontally, the data covers one complete period of Recycler of 11.11 μsec. The top trace in each picture is voltage waveform and the bottom trace is the WCM data.

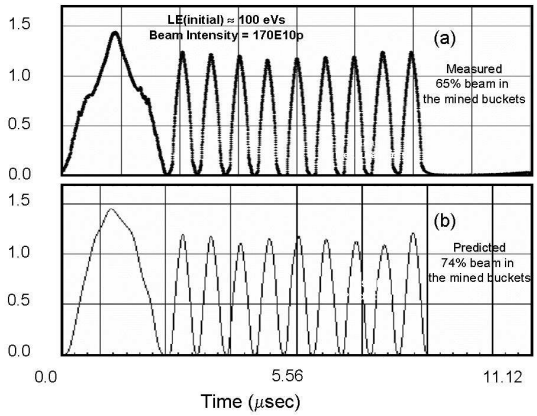


Fig. 13: Measured (top) and the predicted (bottom) line-charge distribution of $170\times10^{10}$ protons after mining.

Fig. 12 shows the experimental demonstration of momentum mining on the proton beam of initial longitudinal emittance ≈ 100 eVs and half energy spread of 13.5 MeV (Fig. 12a). The beam was bound between two barriers of 2 kV each. The barrier separation is about 3 μsec. The goal was to mine about 54 eVs beam from the low emittance region of the phase-space and isolate the rest in a bigger bucket. After mining the low longitudinal emittance beam in nine smaller buckets and the rest in a larger bucket (see Fig.13a), the 9th mini-bunch is moved to extraction region and further divided in to four 2.5 MHz bunches. The Fig.12b shows the beam kept ready for transfer to the down-stream accelerators. The longitudinal emittance of the beam in each of eight mini-buckets is 5.6±0.6 eVs (95% emittance) and that in 2.5 MHz bucket is about 1.5±0.3 eVs. It is important to note that after mining we were able to produce nearly 1) equal intensity and 2) equal longitudinal emittance bunches for each of the nine transfers. This scenario meets all of the antiproton emittance requirements for the Run II at Fermilab.

Fig. 13 shows a comparison between the measurements and the ESME predictions for the WCM data taken soon after mining on the beam shown in Fig.12a. Experimentally, we find that about 65% of the beam particles in the mined bucket and the rest in the left most bucket. ESME predicts about 74% mining efficiency. The difference is due primarily to the difference between energy distributions of assumed ideal parabolic distribution for the initial energy distribution of the un-cooled proton beam used in the demonstration. The experiments carried out later, on the stochastically cooled antiprotons, gave mining efficiency comparable to the predictions.

Recently the electron cooling has become available on the stored antiprotons in the Recycler [31]. Fig. 14 shows the mining data on the e-cooled antiprotons of nearly $300\times10^{10}$ and initial LE≈68 eVs. The mining efficiency was about 98%.

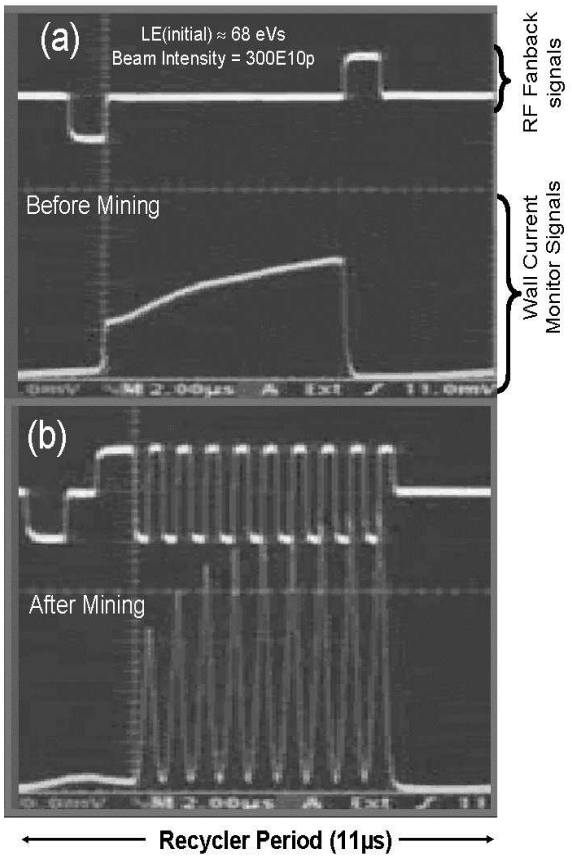


Fig. 14: The experimental data on longitudinal momentum mining on the antiprotons cooled initially with the stochastic cooling and later using electron cooling.

As a final remark, one can think of numerous variations of the method of longitudinal momentum mining described above. In the method presented here we had pre-determined rf pulse widths for mining buckets. The energy spread and LE of mined beam are set by selecting proper barrier pulse height. For example, to mine a 6 eVs beam out of 54 eVs beam we used a barrier bucket of $T_1$ = 0.34 μsec, $T_2$ = 0 μsec and pulse height is slowly increase from 0 V to 690 V. Instead, with a more sophisticated LLRF system one can vary both $T_1$ and pulse heights simultaneously and meet the same requirements.

There is quite a bit of room for further improvements in the way how the mining is carried out. Need to develop a feed-back system to correct the rf voltage wave form to get nice rectangular beam profile as measured by WCM before mining starts, in contrast to the data shown in Fig. 14. The work is in progress.

The longitudinal momentum mining along with the e-cooling in the Recycler has played quite significant role in the recent spectacular success of the collider performance at Fermilab. We were able to inject nearly constant longitudinal emittance and constant high intensity 36 anti-proton bunches <1.5 eVs each to the Main Injector and then to the Tevatron. Since October 2005 we have broken earlier world record on proton-antiproton luminosity of $140\times10^{30}$cm$^{-2}$sec$^{-1}$ a number of times. The highest luminosity achieved so far is about $172\times10^{30}$cm$^{-2}$sec$^{-1}$. Our Run II goal is $270\times10^{30}$cm$^{-2}$sec$^{-1}$, which is primarily limited by total available anti-protons at present.

**c. Production of bright proton bunches [19, 42]**

Producing high intensity low emittance particle bunches at hadron colliders has been one of the major problems for many years. A technique for coalescing several low intensity bunches into a high intensity bunch (using two rf systems with frequency ratio equal to an odd integer) was developed at Fermilab [43] and has been used over the last two decades. A number of alternative techniques have also been studied [44, 45] at other labs.

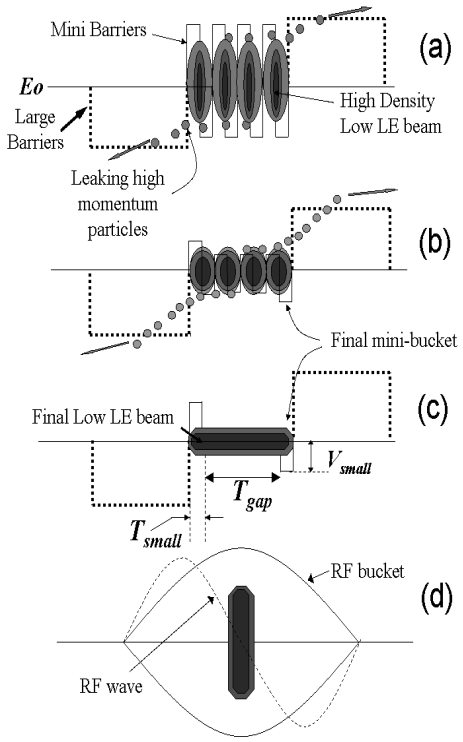


Fig. 15: A schematic of barrier coalescing scheme to produce a bright proton bunch for the Tevatron ppbar collider: a) four bunches in rectangular barrier buckets embedded between two large barriers (anti-bucket), b) intermediate step: pulse heights of mini-buckets are reduced and more particles in high momentum region relative to the synchronous particles are removed, c) low LE beam bunch in a final barrier bucket and d) bunch after rotation in a lower harmonic sinusoidal rf bucket; the rf wave is shown by dashed line.

A year ago, it was realized that the Tevatron proton-antiproton luminosity can be increased significantly by changing the operating point of transverse tunes in the Tevatron at collision and increasing the proton beam brightness [46]. But the currently used proton coalescing technique in the Main injector is quite limited by both in bunch emittance and intensity. Recently, a new method is proposed to produce bright proton bunches for Tevatron operation that uses the broad band rf systems [19, 42]. This method is essentially born out of longitudinal momentum mining discussed earlier.

The principle of the technique is schematically illustrated in Fig. 15. In the example shown here we illustrate four bunch coalescing. This can be extended to larger number of bunches. The proton bunches at Fermilab Booster arrive in 53 MHz structure. These bunches resemble distribution in between Gaussian and parabolic in the ($\Delta$E, $\tau$)-phase space. It is evident that to produce high brightness proton bunches we need to remove the protons in the high momentum tail of the distribution from each bunch and coalesce them without emittance growth. The barrier coalescing involves 1) removing the high momentum particles (Figs. 15a and 15b) by capturing the bunches in barrier buckets of area smaller than the bunches, 2) capture in a larger barrier bucket of matched bucket height (Fig. 15c), 3) finally transfer to an rf bucket which can be accelerated to required energy. In the current scheme, the bunch coalescing is performed above the Main Injector transition energy to eliminate longitudinal emittance growth due to transition crossing.

Beam dynamics simulations have been carried out for the Main Injector parameters to demonstrate the feasibility of the technique. Fig. 16 shows results for eleven bunch barrier coalescing. These bunches arrive from the Booster at 8 GeV into the Main Injector and accelerated to 27 GeV. The transition energy of the Main Injector is about 20.49 GeV. Each of these bunches are about 0.15 eVs. At 27 GeV the voltage of 53 MHz buckets are brought down adiabatically and eventually turned off between nine mini-barrier buckets imbedded between two larger barriers as shown. Once all the high momentum particles are removed from the region of interest, intermittent mini-barriers are eliminated except two (Fig. 16c). The bunch is finally captured in a 53 MHz bucket after a quarter synchrotron rotation in a 2.5 MHz bucket (Fig. 16d) and accelerated to 150 GeV for Tevatron injection.

Simulation results shown above are carried out with beam-loading compensation taken into account. This shows that one can produce proton bunch of intensity in access of $40\times10^{10}$ ppb with longitudinal emittance $\leq$2.2 eVs. We estimate that such bunches can produce about 40% more peak luminosity in the Tevatron as compared with our best performance so far. This luminosity projection assumes half of antiproton stack rate designed for the Run II (design average antiproton stack rate is about 30mA/hour). Presently this scheme is under consideration.

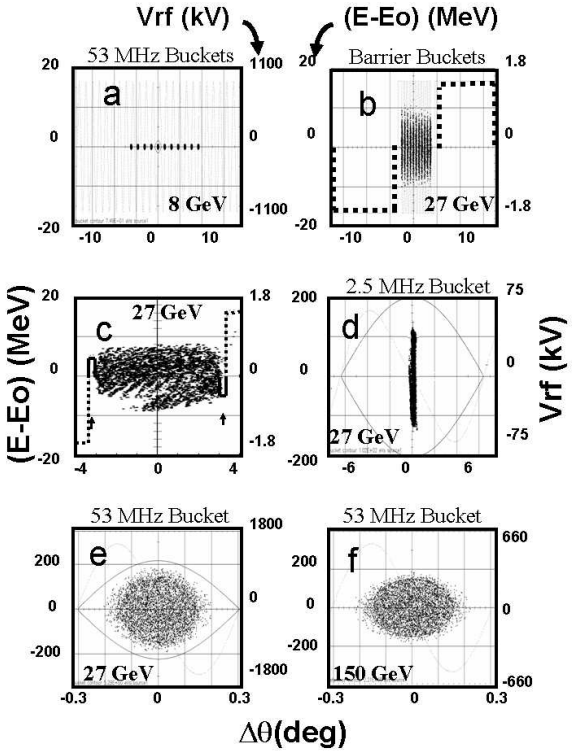


Fig. 16: Simulated phase-space distribution for barrier bucket coalescing scheme using ESME. a) Injection, b) start of barrier coalescing at 27 GeV, c) intermediate step, d) bunch rotation in 2.5 MHz bucket, e)capture in 53 MHz bucket, f) bunch at 150 GeV matched to Tevatron bucket.

**d. Fast Bunch Compression and Cogging [15]**

Recently, a novel method for beam compression and cogging is developed by Bill Foster et. al. [15] using a broad band RF system in circular accelerators. Beam manipulations can be done rapidly, without emittance growth. Here I review the general principle of the methods with some illustrations from our experiments in the Recycler. The technique of bunch compression and cogging explained in Section III are different from that explained here. The previous techniques are too slow and less efficient for some applications.

***i) Fast Bunch Compression***

The principle of fast bunch compression is illustrated in Fig. 17 for two bunches stacked side by side. For a synchrotron with beam injection below transition energy, like the Recycler, the direction of synchrotron motion of the beam particles in a linear bucket is shown in Fig. 17b. The two bunches are allowed to rotate till the net energy spread of the beam its less than the energy acceptance of the synchrotron. At this moment they are made to change

their direction of their rotation as in Fig.17d by changing the slope of the linear rf voltage curve. The binding barriers are continuously moving closer to one another in synchronous to the first and second bunch rotation. As soon as the bunch length reaches its minimum the linear rf wave between the barriers are turned off.

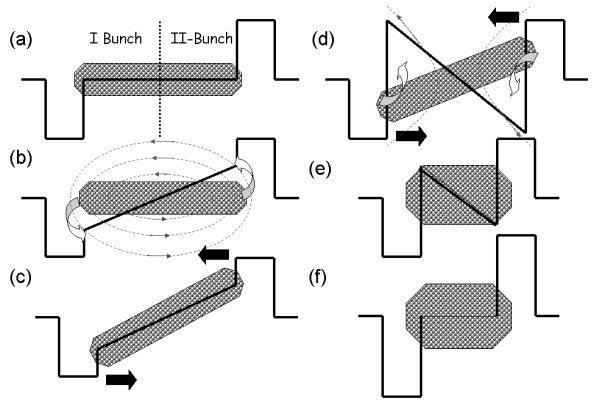


Fig. 17: A schematic view of various stages of fast bunch compression. a) Injection (start), b)introducing a linear ramp c) move the rectangular barriers closer as the bunches rotate, d) flip the linear ramp e) move the rectangular barrier further, f) completion of bunch compression.

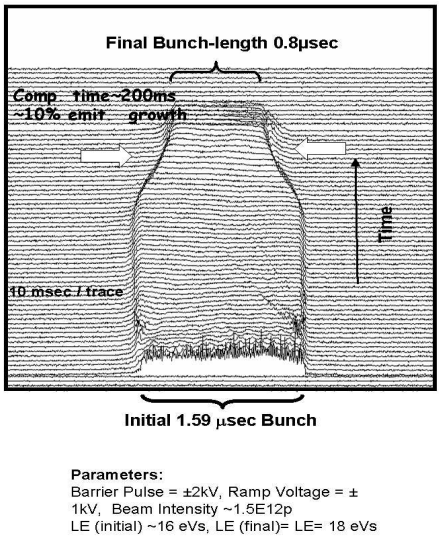


Fig. 18: Experimental mountain range data on bunch compression in the Recycler [15]

The Fig. 18 illustrates an example of a single bunch compression from 1.59μsec to 0.8 μsec in about 180 msec. The compression rate depends on the slope of the linear rf voltage, i.e., on the available rf voltage for bunch rotation. The parameters used for this beam experiment are also shown in the figure. The longitudinal emittance is preserved within the errors of measurements. Beam dynamics simulations of this technique using ESME [47] suggested preservation of longitudinal emittance within a few percent. The case shown here is symmetric bunch compression. We have also tested non-symmetric bunch compression in the Recycler.

Recently, based on our experimental results, a detailed mathematical analysis of this technique has been presented [48], which is consistent with our observation.

### *ii) Bunch stretching*

Fig. 19 shows how one can do fast bunch stretching without emittance growth. The schematic view of the steps involved in this technique is also shown along with experimental data.

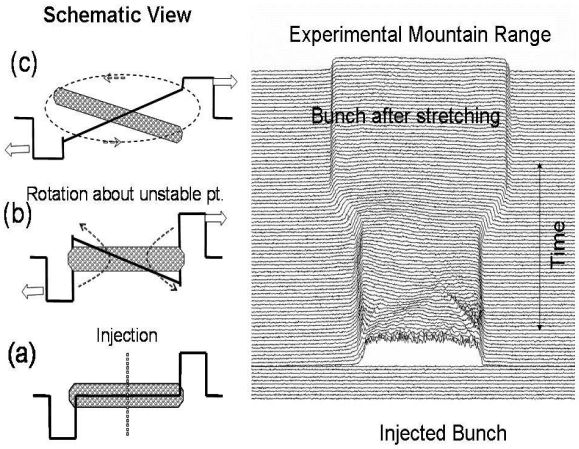


Fig. 19: A schematic view of various stages of fast bunch stretching (left side pictures). a) Injection (start), b) introducing a linear ramp and start moving the rectangular barrier as the bunch rotates, c) flip the linear ramp and complete bunch stretching as soon as bunch lines up. The corresponding data from an experiment [15] is shown on the right side picture.

### *iii) Bunch Cogging*

In the past bunch cogging is performed by slowly changing the rf frequency and phase relative to the bunch. This process has to be carried out adiabatically with a rate smaller than the synchrotron oscillation period of the beam particles. For beam particles in a barrier buckets dealt here have a range of synchrotron oscillation frequency with oscillation frequency equal to zero for synchronous particles. Therefore, in principle, adiabatic bunch maneuvring is impossible by the method explained earlier.

Fast cogging [15] is an elegant method. Fig. 20 shows both schematic views of the steps involved in the process and mountain range from an experiment carried out in the Recycler. A bunch of about 1.59 μsec is moved by about 0.5 μsec in about 150 msec. This corresponds to a cog

rate of about 112 deg /sec if we follow the conventional technique illustrated in Fig. 4 and the longitudinal emittance growth would be quite significant (beam will fall out of the barrier bucket). In the present case a small growth is seen. Theoretically, for a well synchronized motion of the beam and of barrier bucket, one expects no emittance growth, because all particles see same rf acceleration during cogging.

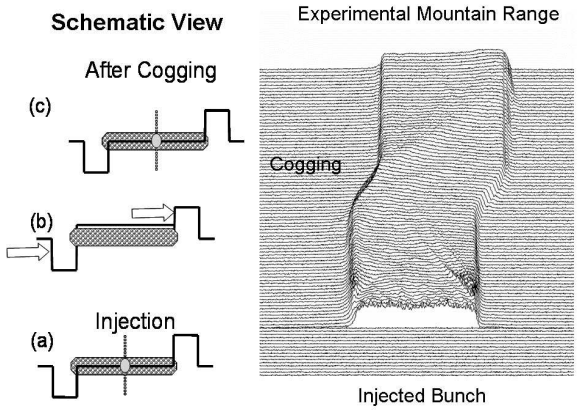


Fig. 20: A schematic view and experimentally measured mountain range of fast cogging [15].

### e. Other Applications of Barrier rf systems at Fermilab

There are a number of other applications of broad band rf system at Fermilab which are helping to control instability of the beam in accelerators and storage rings. New high intensity proton stacking method based on barrier rf system are also proposed. Some of them are listed below.

a. High Intensity protons for the NuMI operation of the Main Injector
   - MI longitudinal dampers [20, 49] ← in use
   - Confining leaking beam during slip-stacking and Injection gap clearing for NuMI operation [50],
   - Momentum stacking [51]← Studies are scheduled in summer 2006

b. Recycler Applications
   - Gated stochastic cooling in the Recycler [52]← Demonstrated
   - Besetting the beam instability in the Recycler with sweeping anti-barrier bucket [53] ←proposed
   - Ion clearing gap with barrier rf system← in use at the Recycler and Accumulator

## V ISSUES

It is important to note that every barrier rf system has an intrinsic shunt impedance. As a result of this, the cavity beam loading becomes an issue in use of the barrier rf system at high intensities. A first observation of potential well distortion [25] of barrier beam in hadron ring is made at Fermilab Recycler. This certainly makes the acceleration of high intensity super-bunches in synchrotrons more difficult than originally thought. Hence, is essential to develop a beam-loading compensation system as an integral part of barrier rf system used for any high intensity operation.

The distortion of the line charge density due to beam loading at the Recycler is illustrated in Fig 14a. We have seen this effect at as low as $20\times10^{10}$ particle in a bunch of 1.6μsec long. The uneven distribution of the cooled beam particles has leads to uneven bunch intensities for Tevatron injection. This has posed additional complexity in evaluating bunch by bunch luminosity at the Tevatron.

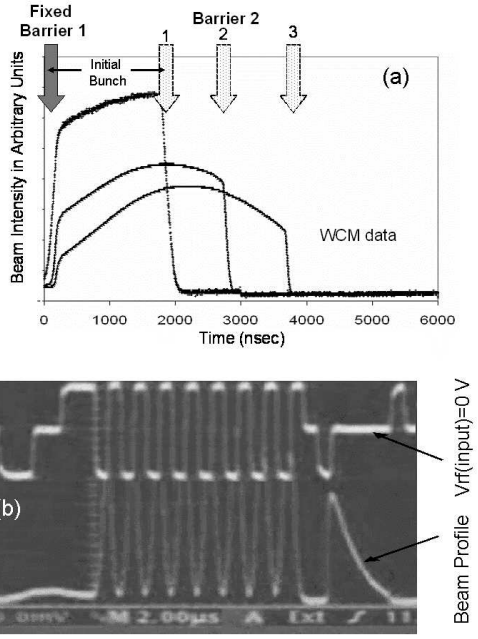


Fig. 21: Experimental a) WCM data on stored beam of $120\times10^{10}$ particle. The barrier gap ($T_2$) is varied slowly by moving "Barrier-2" from 1 to 2 to 3. The change in beam profile indicates change in the harmonic components between two barriers as a function of the barrier positions. b) Effect of presence of multiple barriers on a bunch

Other issues with barrier rf is related to the distortion of the waveform due to higher harmonic components. Fig. 21 shows two such cases. In Fig. 21a, a beam of about $120\times10^{10}$ particle is captured in a 1.6 μsec barrier bucket and expanded slowly to 2.4 μsec and then to 3.4 μsec. During this experiment no other barrier rf wave were present in the ring. Simply by relocating the "barrier pulse 2" relative to Barrier-1 resulted in a noticeable effect on the line charge distribution, which indicated change in harmonic components between barriers. In ideal case this region should be free of any rf voltage. We saw as high as about 1% of the peak rf voltage in the region of zero rf voltage.

Fig. 21b illustrates a case of effect of higher harmonic component due to presence of other rf wave elsewhere in the ring.

These effects become more sever for colder antiproton beam. Currently some effort is in progress to correct these problems in the Recycler.

## VI SUMMARY AND CONCLUSIONS

The use of barrier rf technology in accelerator is relatively new. A number of accelerators at Fermilab are equipped with barrier rf systems and new applications are invented. Some of the techniques are critical for recent high intensity proton beam acceleration in the Main Injector and high proton-antiproton luminosity performances at the Tevatron. The broad band rf system in the Recycler has opened doors for several innovative developments in the field of accelerator physics. Longitudinal momentum mining, longitudinal phase space coating, new methods for bunch compression and cogging are a few such examples. Adopting longitudinal momentum mining in the e-cooled antiproton has helped us to increase proton-antiproton luminosity by a factor of nearly three. We are investigating the possibilities of using fast bunch compression technique in doubling the 120 GeV proton beam intensity for our neutrino program, like NuMI and other fixed target HEP experiments. I am quite confident that there are a number of interesting applications yet to be invented at accelerator lab with barrier systems and use them to improve accelerator performance and to understand beam dynamics.

I would like to thank many individuals in the Fermilab Accelerator Division - D. Wildman, , G. W. Foster, C. Gattuso, B. Chase, J. MacLachlan, J. Marriner, D. Neuffer and K. Ng, for their help and discussions during various stages of this work. I also acknowledge the help of K. Seiya and J. A. P. Varghese during the experiments on fast bunch compression and cogging presented here. I would like to thank Pushpa Bhat and Vincent Wu for their comments on this paper.

## REFERENCES

[1] Design Report Tevatron 1 Project http://library.fnal.gov/archive/design/fermilab-design 1984-01.shtml.
[2] J.E. Griffin *et al.,* IEEE, Trans. Nucl., Sci., NS-30, 3502 (1983).
[3] K. Takayama et. al., Phy. Rev. Lett. 8 (2002) 144801-1; Recent results in this proceedings.
[4] G. Jackson, Fermilab-TM-1991, November, 1996.
[5] Y. Shimosaki *et al.,* PRST Vol. 7, 014201 (2004).
[6] M. Blaskiewicz *et., al.,* Proc. of PAC99, New York, page 2280.
[7] M. Fujieda PAC99, page 857.
[8] T. Bohl, Proc. EPAC2000, 1220.
[9] C.M. Bhat, Proceedings of 20th ICFA Advanced Beam Dynamics Workshop on High Intensity and high brightness hadron beams, Batavia IL, (April 2002), AIP Vol. 642, 229.
[10] C. M. Bhat, PAC2003, p 2345.
[11] H. Kang, et. al., PAC2003, p 3180.
[12] A. Cadorna, et. al., PAC2003, p2348.
[13] C.M. Bhat and J. Marriner, PAC2003, p 514.
[14] C.M. Bhat and K. Y. Ng, (to be published in Proc. of Factories 2003, Stanford, California, October, 2003). FERMILAB-CONF-03-395-T (Oct 2003).
[15] G.W. Foster et. al., Proc. of EPAC2004, 1479.
[16] C.M. Bhat, Phys. Letts. A 330 (2004) 481-486.
[17] C.M. Bhat, Proc. of EPAC2004, page 236.
[18] C.M. Bhat, PAC2005, p 1093.
[19] C.M. Bhat, PAC2005, p 1745.
[20] G. W. Foster et al., PAC2003, p 323 .
[21] J.E. Dey and D.W. Wildman, PAC1999, p 869.
[22] W. Chou *et al.,* PAC2003, p 2933.
[23] "Fermilab Main Injector Technical Design Handbook" (Internal Report, 1994).
[24] S.Y. Lee and K. Y. Ng, Phys. Rev. E, Vol. 55, 5992 (1997); S. Y. Lee, *Accelerator Physics*, 1st edition (World Scientific, Singapore, 1999), Chap. V, p.305.
[25] C.M. Bhat and K.Y. Ng, FERMILAB-CONF-03-395-T (Oct 2003); Factories 2003, Stanford, California, October 13-16, 2003.
[26] B. Fellenz and J. Crisp (private communications).
[27] Ming-Jen Yang, (unpublished, console applications program for RTD720, 2000); R. West and C.M. Bhat, (unpublished, console applications program for LeCroy Scope, 2003).
[28] D. Boussard – CERN SPS/86-11(ARF), Geneva 1986.
[29] R. Pasquinelli *et al*., PAC2003, p 3068.
[30] "Energy Spread and Emittance of a Beam in the Recycler," V. Balbekov, Fermilab, Beams-doc-1077-v1, Jan. 2004.
[31] S. Nagaitsev, et al., Phys. Rev. Lett. 96:044801 (2006).
[32] J. A. MacLachlan, HEACC'98, XVII International Conference on High Energy Accelerators, Dubna, 184, (1998); J. A. MacLachlan, Fermilab Report No FN-529, (1989) (Unpublished); (private communications 2004); The latest version of the code is available at http://www-ap.fnal.gov/ESME/.
[33] B. Chase et al, Proc. on the 1997 Int. Conf. on Accel. and Large Experimenatal Physics Control Systems, Beijing, China (1997).
[34] "A First Look at the Longitudinal Emittance in the Fermilab Recycler Ring," C.M. Bhat, MI Note 287 (Aug. 2002).
[35] Stan Pruss, and Guan Wu (private communications, 2003).
[36] "Fermilab Collider Run II: Accelerator Status and Upgrades", P. C. Bhat and W. J. Spalding, to be published in the Proceedings of the 15th Topical

Conference on Hadron Collider Physics 2004, American Institute of Physics.
[37] J. Marriner and C.M. Bhat, (pbar stacking in the Recycler, unpublished, 2002).
[38] B. Chase, P. Joireman and C. Gattuso (private communications, 2006).
[39] 'Pbar stacking in the Recycler: Longitudinal Phase-Space Coating", C.M. Bhat, Beams-Doc-2057-V1, December 2005.
[40] J. MacLachlan, FERMILAB-Conf-00/117, June 2000.
[41] Y.Y. Lee et al, LINAC2002, Gyeougju, Korea, (2002), page 67.
[42] C.M. Bhat, Fermilab-FN-0761 (2004).
[43] J. E. Griffin, J. A. MacLachlan and Z. B. Qian, IEEE, Trans. Nucl., Sci., **NS-30**, No. 4, (1983) 2627.
[44] J. M. Brennan et al, Proc. of EPAC2004, Lucerne, Switzerland (2004) p 905.
[45] H. Damerau and R. Groby, Proc. of EPAC2004, Lucerne, Switzerland (2004) p 1852.
[46] V. Shiltsev, Beams-Doc-2016-v1 and Beams-Doc-1876-v1 page 10.
[47] J. MacLachlan (private communications, 2003).
[48] K. Y. Ng, Fermilab-FN-0742 (2004).
[49] P. Adomson et. at., PAC2005, p 1440.
[50] C. M. Bhat and D. Wildman, private communications; W. Chou et al., PAC2005, p1189.
[51] J. Griffin, Private communications, 2003 (K. Ng., AIP Conf.Proc.642:226-228, 2003 and FERMILAB-TM-2183 (Sep 2002), theoretical analysis of J. Griffin's proposal).
[52] D.R. Broemmelsiek, et. al., EPAC04, p794.
[53] C.M. Bhat (unpublished, 2005).